Theoretical study of liquid-immersed exposed-core microstructured optical fibers for sensing

S. C. Warren-Smith*, S. Afshar V., and T. M. Monro

Centre of Expertise in Photonics, School of Chemistry & Physics, The University of Adelaide, Adelaide, SA 5005, Australia
**Corresponding author: stephen.warrensmith@adelaide.edu.au*

Abstract: The absorption and fluorescence sensing properties of liquid-immersed exposed-core microstructured optical fibers are explored for the regime where these structures act as supported nanowires with direct access to the sensing environment. For absorption-based sensing we demonstrate that the amount of power propagating in the sensing region of the exposed-core fiber can compete with that of traditional MOFs. For fluorescence-based sensing, we see that in addition to the enhanced fluorescence capture efficiency already predicted for small-core, high refractive index contrast fibers, an improvement of up to 29% can be gained by using liquid-immersed exposed-core fibers. Additionally, calculation of the losses associated with interfaces between filled and unfilled sections predict significant benefit in using high refractive index substrate glasses for liquid-immersed exposed-core fiber sensing. This work demonstrates that, for fiber dimensions of interest, the exposed-core fiber is an attractive new sensor technology.

OCIS codes: (060.2370) Fiber optics sensors; (060.4005) Microstructured fibers; (300.1030) Absorption; (300.2530) Fluorescence, laser-induced.

References and links

1. G. Stewart and B. Culshaw, "Optical waveguide modelling and design for evanescent field chemical sensors," Opt. Quantum Electron. **26**, s249-s259 (1994).
2. J. B. Jensen, P. E. Hoiby, G. Emiliyanov, O. Bang, L. H. Pedersen, and A. Bjarklev, "Selective detection of antibodies in microstructured polymer optical fibers," Opt. Express **13**, 5883-5889 (2005).
3. L. Rindorf, P. E. Hoiby, J. B. Jensen, L. H. Pedersen, O. Bang, and O. Geschke, "Towards biochips using microstructured optical fiber sensors," Anal. Bioanal. Chem. **385**, 1370-1375 (2006).
4. C. M. B. Cordeiro, M. A. R. Franco, G. Chesini, E. C. S. Barretto, R. Lwin, C. H. B. Cruz, and M. C. J. Large, "Microstructured-core optical fibre for evanescent sensing applications," Opt. Express **14**, 13056-13066 (2006).
5. Y. Zhu, H. Du, and R. Bise, "Design of solid-core microstructured optical fiber with steering-wheel air cladding for optimal evanescent-field sensing," Opt. Express **14**, 3541–3546 (2006).
6. T. Ritari, J. Tuominen, H. Ludvigsen, J. C. Petersen, T. Sorensen, T. P. Hansen, and H. R. Simonsen, "Gas sensing using air-guiding photonic bandgap fibers," Opt. Express **12**, 4080-7 (2004).
7. Y. L. Hoo, W. Jin, C. Z. Shi, H. L. Ho, D. N. Wang, and S. C. Ruan, "Design and modeling of a photonic crystal fiber gas sensor," Appl. Opt. **42**, 3509-3515 (2003).
8. C. M. B. Cordeiro, E. M. dos Santos, C. H. Brito Cruz, C. J. de Matos, and D. S. Ferreiia, "Lateral access to the holes of photonic crystal fibers – selective filling and sensing applications," Opt. Express **14**, 8403-8412 (2006).
9. C. M. B. Cordeiro, C. J. S. de Matos, E. M. dos Santos, A. Bozolan, J. S. K. Ong, T. Facincani, G. Chesini, A. R. Vaz, and C. H. Brito Cruz, "Towards practical liquid and gas sensing with photonic crystal fibres: side access to the fibre microstructure and single-mode liquid-core fibre," Meas. Sci. Technol. **18**, 3075-3081 (2007).
10. C. J. Hensley, D. H. Broaddus, C. B. Schaffer, and A. L. Gaeta, "Photonic band-gap fiber gas cell fabricated using femtosecond micromachining," Opt. Express **15**, 6690-6695 (2007).
11. A. van Brakel, C. Grivas, M. N. Petrovich, and D. J. Richardson, "Micro-channels machined in microstructured optical fibers by femtosecond laser," Opt. Express **15**, 8731-8736 (2007).
12. F. M. Cox, R. Lwin, M. C. J. Large, and C. M. B. Cordeiro, "Opening up optical fibres," Opt. Express **15**, 11843-11848 (2007).

13. T. M. Monro, H. Ebendorff-Heidepriem, Patent Application, 'Fabrication of nanowires' (PCT/AU2006/00501), October 2005.
14. H. Ebendorff-Heidepriem, P. Petropoulos, S. Asimakis, V. Finazzi, R. C. Moore, K. Frampton, F. Koizumi, D. J. Richardson, and T. M. Monro, "Bismuth glass holey fibers with high nonlinearity," Opt. Express **12**, 5082–5087 (2004).
15. M. J. Steel, T. P. White, C. M. de Sterke, R. C. McPhedran, and L. C. Botten, "Symmetry and degeneracy in microstructured optical fibers," Opt. Lett. **26**, 488-490 (2001).
16. G. S. Wiederhecker, C. M. B. Cordeiro, F. Couny, F. Benabid, S. A. Maier, J. C. Knight, C. H. B. Cruz, and H. L. Fragnito, "Field enhancement within an optical fiber with a subwavelength air core," Nat. Photonics **1**, 115-118 (2007).
17. N. Ganesh and B. T. Cunningham, "Photonic crystal enhanced fluorescence," in *Tech. Digest*, (Opt. Soc. Am., 2007) p. CThz5.
18. J. Lou, L. Tong, and Z. Ye, "Modeling of silica nanowires for optical sensing," Opt. Express **13**, 2135-2140 (2005).
19. S. Afshar V., S. C. Warren-Smith, and T. M. Monro, "Enhancement of fluorescence-based sensing using microstructured optical fibres," Opt. Express **15**, 17891-17901 (2007).
20. Y. Ruan, E. P. Schartner, H. Ebendorff-Heidepriem, P. Hoffmann, and T. M. Monro, "Detection of quantum-dot labeled proteins using soft glass microstructured optical fibers," Opt. Express **15**, 17819-17826 (2007).
21. A. W. Snyder and J. D. Love, *Optical Waveguide Theory* (Chapman and Hall, 1995).
22. Agrawal, *Nonlinear Fiber Optics* (Academic Press, 2007).
23. F. W. D. Rost, *Fluorescence Microscopy* (Cambridge University Press, 1992).
24. M. Sumetsky, Y. Dulashko, and A. Hale, "Fabrication and study of bent and coiled free silica nanowires: Self-coupling microloop optical interferometer," Opt. Express **12**, 3521-3531 (2004).
25. J. D. Love and C. Durniak, "Bend loss, tapering, and cladding-mode coupling in single-mode fibers," IEEE Photon. Technol. Lett. **19**, 1257-1259 (2007).
26. N. H. P. Kao, N. Yang, and J. S. Schoeniger, "Enhancement of evanescent fluorescence from fiber-optic sensors by thin-film sol-gel coatings," J. Opt. Soc. Am. A **15**, 2163-2171 (1998).
27. W. Henry, "Evanescent field devices: a comparison between tapered optical fibers and polished or D-fibers," Opt. Quantum Electron. **26**, s261-s272 (1994).
28. A. Cargama, "Modal analysis of coupling problems in optical fibers," IEEE Trans. Microwave Theory Tech. **MTT-23**, 162-169 (1975).
29. C. Vassallo, "On a rigorous calculation of the efficiency for coupling light power into optical waveguides," **QE-13**, 165-173 (1977).
30. M. Mostafavi, I. Itoh, and R. Mittra, "Excitation of an optical fiber by a Gaussian beam," Appl. Opt. **14**, 2190-2193 (1975).
31. J. A. Buck, *Fundamentals of Optical Fibers* (John Wiley & Sons, 2004).
32. C. Vassallo, *Optical waveguide concepts* (Elsevier 1991).
33. D. Marcuse, "Radiation losses of tapered dielectric slab waveguides," Bell Syst. Tech. J. **49**, 273-290 (1970).
34. P. A. Wallace, M. Campbell, Y. Yang, A. S. Holmes-Smith, and M. Uttamlal, "A distributed optical fibre fluorosensor for pH measurement," J. Lumin. **72-74**, 1017-1019 (1997).

1. Introduction

Microstructured optical fibers (MOFs) can be used to dramatically improve traditional absorption and fluorescence-based fiber sensors due to the ability to precisely control their optical characteristics. In particular, this control can be used to increase the amount of optical power that is available to interact with the environment that is to be sensed [1-4], and reported overlap values between the guided modes and the materials within the holes of the fiber include 6.5% for a multi-core MOF [3], 40% for a nanowire [5], and 97% or higher for an air-core photonic bandgap fiber [6]. However, these sensors require that the chemicals to be measured are located within the holes of the MOF, and generally require filling the fiber with liquids or gases. Although this approach delivers high sensitivity due to the possibility of integrating the response over the fiber length, when used in this manner, MOF-based sensors do not lend themselves to distributive sensing. In 2003 Hoo, *et al.*, proposed the introduction of periodic openings along a sensing fiber that allow access to the fiber's core [7]. Fabrication has subsequently been demonstrated by the use of a fusion splicer and air pressure to blow holes within an MOF [8], use of a focused ion beam [9], and femtosecond laser micromachining [10, 11]. Cox, *et al.*, have also demonstrated that by creating the fiber opening at the preform stage of the fiber fabrication longer lengths of exposed-core fiber can be fabricated, such as by drilling a slit into the cladding of a polymer MOF preform [12]. This exposed-core design of optical fiber sensor has advantages over other fiber based sensors such as fast-response, real-time sensing with no requirement for selective hole filling. Potential

implementations include long interaction length point sensing by use of a coiled sensing cell, multipoint sensing, and continuous distributive sensing via optical time domain reflectometry techniques.

In this paper we present the first theoretical study of the characteristics of this class of optical fiber for the case where the exposed section is immersed in a liquid for the purpose of intensity-based absorption or fluorescence sensing. The particular fiber geometry studied has a wavelength-scaled (nanowire-like) core suspended within a robust jacket that has a missing segment (or wedge); see Fig. 1(c) [13]. This geometry is as close as practically possible to the ideal case of a nanowire suspended in air (or within an environment to be sensed). From a theoretical point of view it is essentially a wagon wheel (WW) fiber (Fig. 1(a) and Fig. 1(b)) [14] (or steering wheel fiber [5]), but where one of the holes has been filled with a sensing material (the exposed section) while the others remain filled with air. If the filling material has unity refractive index (air) then the modal characteristics of the fiber are unchanged by the introduction of the wedge within the fiber jacket. When a portion of the fiber is immersed in a liquid, the mode profile spreads out into the exposed section due to the weaker confinement resulting from the raised refractive index of the liquid (for a water-based solution, n=1.33).

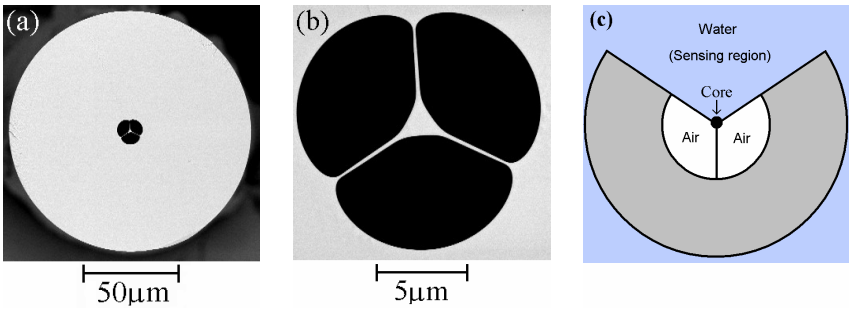

Fig. 1. Scanning electron microscope (SEM) image of an F2 (lead-silicate), wagon wheel fiber (a) and its core region (b). This fiber forms the basis of the exposed-core fiber where one of the holes is opened up to allow it to be accessible to the external environment, as shown in the schematic diagram (c).

Here we evaluate the absorption and fluorescence sensing performance for a range of fibers of this type, and compare the results to those obtained with fully filled WW fibers. The losses associated with the mode mismatch that occurs at the liquid boundaries within an exposed-core fiber are also considered. This comparison allows us to determine the feasibility of using exposed-core fibers within sensing systems, and to evaluate the impact of using an asymmetrically raised refractive index profile.

2. Numerical modeling

The field distributions corresponding to the pair of fundamental guided modes of the fiber were determined using the commercially available finite element modelling package COMSOL 3.2. For the case where all three surrounding holes are filled with water there is a three-fold rotational symmetry and hence two degenerate fundamental modes are found (to within the numerical accuracy of the model – see Sec. 3) [15]. However, when just one hole contains a liquid, as in the case of an exposed-core fiber, there is only one reflection axis of symmetry and the modes are no longer degenerate. Instead, the first two modes exhibit strong birefringence, with one mode being polarized essentially parallel to the axis of symmetry and the other orthogonal to this.

Figure 2 shows two example fundamental field distributions of a liquid-immersed exposed-core fiber for a low refractive index host material (silica, n=1.46) and a high refractive index glass host (bismuth, n=2.09). Arrows indicate the direction of the electric field and the field profile shown is the z-component of the Poynting vector. The core sizes are defined as the diameter of a circle whose area is equal to a triangle that fits wholly within the core. The core diameters were chosen so that the effective areas are located at approximately

equivalent locations on their respective effective area versus core diameter curves in order to allow comparison of their properties (see Sec. 3). The core diameters are 0.505μm for silica and 0.17μm for bismuth, resulting in effective areas of 0.76μm^2 for silica and 0.24μm^2 for bismuth at a wavelength of 590nm. In each case, the first fundamental mode is approximately linearly polarized with the direction of polarization parallel to the axis of symmetry, and exhibits a high intensity peak in the sensing region at the refractive index boundary. The higher refractive index material (bismuth in this case) exhibits greater confinement, as seen by the smaller dimensions of the bismuth fiber core, and thus has a greater high intensity peak at the boundary. This thin-layer high intensity peak has previously been investigated by other authors [16-18] and we shall see that it is beneficial for fluorescence sensing applications [19]. Note that only the mode with polarization parallel to the axis of symmetry has a high intensity peak in the sensing region for the exposed core fiber, and we will see this leads to significant differences in the relative fluorescence capture into each of the fundamental modes.

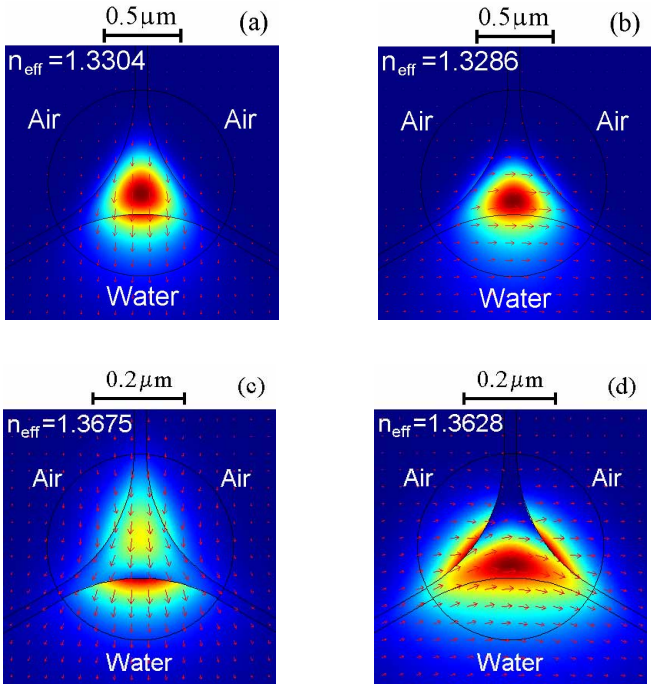

Fig. 2. Fundamental field distributions of a water-immersed exposed-core WW fiber where the substrate glass is silica with a core diameter of 0.505μm (a, b) and bismuth with a core diameter of 0.17μm (c, d). The first (a, c) and second (b, d) fundamental modes are shown for each glass type. The effective index of each mode is shown, which relates to the propagation constant (β) and the wavenumber (k) via $n_{eff}=\beta/k$.

3. Modal properties

First we consider the birefringence of the fundamental modes of the exposed-core fiber, which result from the non-degenerate solutions of this asymmetric geometry. Figure 3 shows the numerical results for the birefringence (Δn) of the exposed-core liquid-immersed fiber as compared with the case where all three holes are filled (the 3-fold symmetric case). We have chosen to consider a wavelength of 590nm as this is close to the fluorescence wavelength of many organic dyes (e.g. rhodamine B). Later, in Sec. 5, a wavelength of 532nm is used as the excitation wavelength in order to match sources used in typical experiments [20], noting that the following results are not qualitatively dependant on the exact choice of wavelength. A range of host glasses have been considered (silica = 1.46, lead silicate (F2) = 1.62, and

bismuth = 2.09) to understand the effect of varying refractive index while still considering realistic materials.

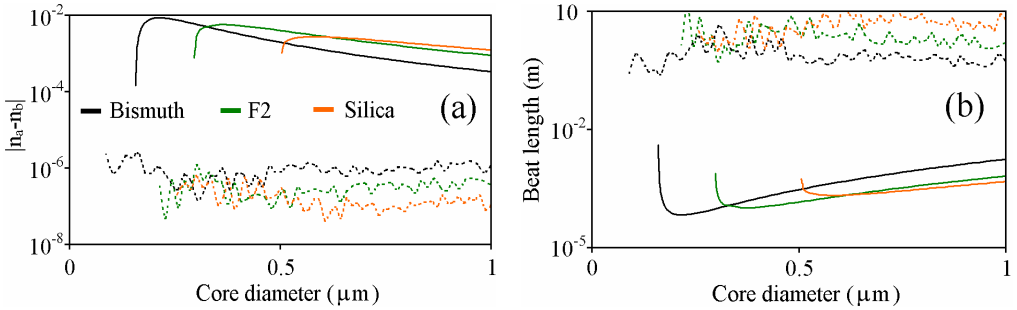

Fig. 3. (a). Difference in effective index between the two degenerate fundamental modes of a fully filled WW structured MOF (dashed lines) and the two fundamental non-degenerate modes of the exposed-core WW (solid lines) for three substrate glasses (indicated in legend). (b). The corresponding beat lengths.

Unsurprisingly, the exposed-core fiber experiences significant birefringence, and it is particularly strong in the small core regime (c.f. wavelength). For example, the predicted beat length can be as short as 68μm for a bismuth exposed-core fiber with a core diameter of 0.2μm. The low-level birefringence that is numerically calculated for the fully filled case is purely the result of numerical errors, which are introduced by the use of a mesh in the finite element modeling [15]. The birefringence measured in this case is thus a measure of the numerical accuracy for this particular geometry and mesh density (~120,000 mesh elements were used) and show that the effective index calculation is accurate to approximately six decimal places. At this point we note that while the value of the birefringence itself does not relate directly to the sensing properties of the exposed core fiber, we will now see that the non-degeneracy of the fundamental modes has consequences on the absorption and fluorescence sensing characteristics.

In order to understand the performance of sensors based on these fibers we evaluated the modal power fraction (PF) [21] within the sensing region and the effective modal area (A_{eff}), which is defined here as the vectorial equivalent to the traditional definition of A_{eff} [22]. Vectorial definitions were used because the weak guidance approximation is inappropriate for microstructured optical fibers where a large difference in refractive index exists between the core and cladding materials. The definitions are;

$$A_{eff,j} = \frac{|\int_{A_\infty} s_{z,j}(\vec{r})dA|^2}{\int_{A_\infty} |s_{z,j}(\vec{r})|^2 \, dA}; \quad (1)$$

$$PF_j = \frac{\int_H s_{z,j}(\vec{r})dA}{\int_{A_\infty} s_{z,j}(\vec{r})dA} \quad (2)$$

where A_∞ is defined to be the infinite transverse cross section, *H* refers to integrating over the sensing region (the water containing hole(s)), *j* is the mode index, and $s_z(\mathbf{r})$ is the *z*-component of the Poynting vector. Figure 4 shows numerical results for these quantities evaluated for the parameters considered previously.

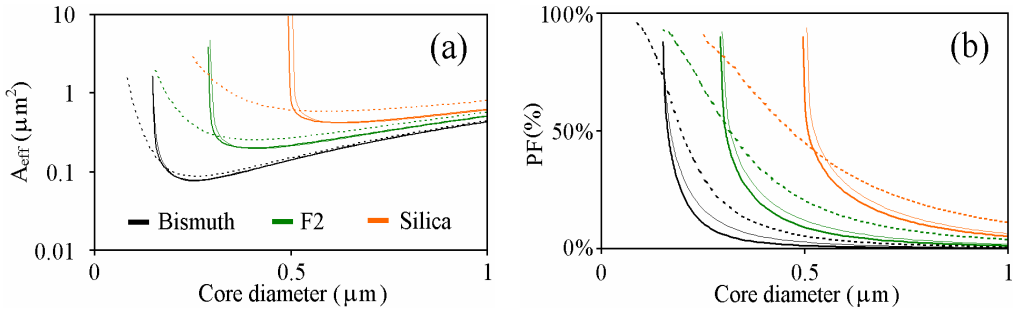

Fig. 4. Effective modal area (a) and modal power fraction (b) as a function of core diameter for three substrate glasses (indicated in legend) where the fiber is either fully filled with water (dashed) or is an exposed-core fiber with one hole containing water (solid). The thick solid lines refer to the fundamental mode of the exposed-core fiber that is polarized parallel to the axis of symmetry and the thin line is for the fundamental mode polarized in the orthogonal direction.

Figure 4(a) shows that for sufficiently large core diameters, the effective area of the exposed-core MOF is less than that for the fully filled case. This is unsurprising because air-glass boundaries provide stronger light confinement than water-glass boundaries. However, as the core size is reduced to subwavelength values, the effective mode area increases rapidly for the exposed-core fiber as the mode spreads dramatically into the water-filled hole.

In a Beer's law [23] absorption sensor the level of absorption is proportional to the available excitation power, shown in Fig. 4(b). Hence, by considering Fig. 4(b) we see that, in spite of utilizing only one out of the three cladding holes, the same absorption sensor performance can be gained for an exposed-core fiber compared to a fully filled fiber. This occurs at a core diameter of approximately 0.52μm for silica fibers (PF = 42%) and 0.15μm for bismuth fibers (PF = 70%), assuming the mode with polarization parallel to the axis of symmetry is used. It should be noted that there are limitations on how small a core size can be used such as coupling losses between filled and unfilled sections of fiber (see Sec. 5), and bend loss [24, 25].

The effects of birefringence on the sensing properties can also be seen in this data: the non-degenerate field distributions now exhibit slightly different power fractions, and hence there is a preferred direction of input coupling polarization that maximizes the power fraction. For an absorption sensor it is preferential to input couple with light polarized orthogonal to the axis of symmetry with a relative difference of 21% for silica fibers and 15% for Bismuth fibers for the core diameters considered above.

4. Fluorescence sensor performance

4.1 Theory

The model described in [19] has here been used to predict the fluorescence capturing ability of the exposed-core fiber. This approach employs the full vectorial solutions of Maxwell's equations and is therefore suitable for MOFs with wavelength-scale features and a high refractive index contrast between the core and cladding regions, unlike previous models that rely on ray-optics [26] or scalar electromagnetic fields [27]. For simplicity we now consider this model for the special case of an attenuation-free fiber of infinite length, which is filled with a solution containing a fluorescent species. In this way the theory describes the fundamental limit on the fluorescence capture possible for the sensor design, and does not depend on which end of the fiber the fluorescence is measured (forwards or backwards fluorescence propagation). Taking into account these assumptions and including the potential for fluorescence capture into multiple non-degenerate modes; the fluorescence capture fraction (FCF) from excitation mode j into modes at the fluorescence wavelength (labeled ν) is given by;

$$FCF_j = \sum_{\nu} \left[\frac{NOI_{j\nu}}{A_{eff,F_\nu}} \right] \frac{\xi \lambda_F{}^2}{16\pi (n_F^H)^2} \tag{3}$$

$$NOI_{j\nu} = n_F^H \left(\frac{\varepsilon_0}{\mu_0} \right)^{1/2} \left[\frac{\int_{A_\infty} |s_{F_\nu}(\vec{r})| dA}{\int_H s_{E_j}(\vec{r}) dA} \right] \left[\frac{\int_H |\vec{e}_{F\nu}|^2 s_{E_j}(\vec{r}) dA}{\int_{A_\infty} |s_{F_\nu}(\vec{r})|^2 dA} \right] \tag{4}$$

where n^H is the refractive index of the fluorescent region, λ_F is the fluorescence wavelength, ξ is the fluorophore efficiency, ***s(r)*** is the z-component of the Poynting vector, and *H* refers to integrating over the fluorophore-filled cross-section. *E* and *F* refer to the excitation and fluorescence wavelengths, respectively. In this loss-free case, FCF has two key terms: a normalized overlap integral (labeled NOI) and the effective area at the fluorescence wavelength, which are dependant on transverse properties of the fiber such as the geometry, refractive index profile, and fluorophore position. The optimization of NOI and A_{eff} is the key to achieving large fluorescence capture within MOF sensors. For example, the effective area can be reduced by moving to smaller core fibers with strong confinement, which we shall see is effective in increasing FCF. It is important to note that NOI in not directly proportional to the power fraction, but is a somewhat more complex expression. This highlights that power fraction alone cannot be used to optimize fluorescence-based optical fiber sensors.

4.2 Fundamental FCF numerical results

FCF was determined for the same glass materials as in Sec. 2, an excitation wavelength of 532nm, and a fluorescence wavelength of 590nm. For simplicity, the input excitation is taken to be a linearly polarized source, and we assume that this excites a single degenerate mode in the fully filled case and a mode with polarization parallel to the axis of symmetry in the exposed-core case. Fluorescence capture into both fundamental modes is then calculated, and the results are shown in Fig. 5(a).

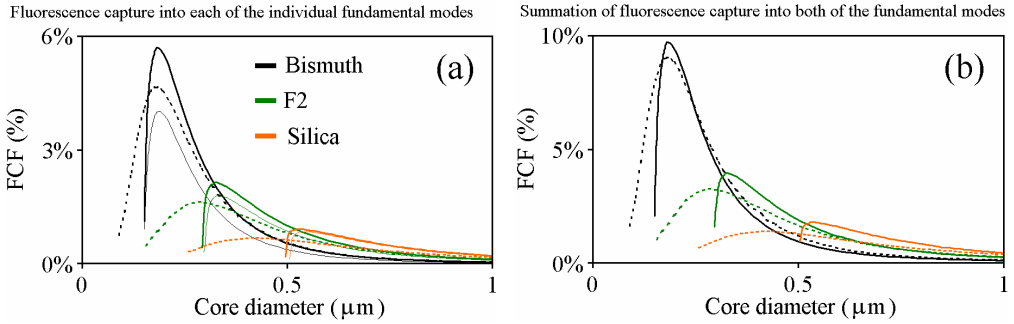

Fig. 5. FCF as a function of core diameter for three substrate glasses (indicated in legend), where the fiber is either fully filled with water (dashed) or is an exposed-core fiber with one hole containing water (solid). In (a) the thick solid lines refer to the fundamental mode of the exposed-core case that is polarized parallel to the axis of symmetry and the thin line is for the fundamental mode with orthogonal polarization. In (b) the result for each fundamental mode has been added to produce the net effect where the thick line refers to the exposed-core fiber and the dashed line is for the fully filled fiber.

The first observation is that for small core diameters, the higher refractive index fibers offer an enhanced fluorescence capture due to the formation of a thin, high-intensity layer at the core-cladding boundary that acts to confine the excited fluorescence near the core, as previously reported [19]. Equation (3) shows that the reduced effective area for high index

glasses is largely responsible for this effect and shows that high-index soft glasses such as F2 and bismuth are attractive materials for MOF sensors provided that small core dimensions are used. Figure 5(a) also shows how FCF changes for an exposed-core fiber where higher peak values can be observed for the fluorescence capture (and this achieved at slightly larger core diameters). We also see a dramatic difference in capture into each of the two non-degenerate fundamental modes, particularly for the high refractive index fibers. For example, the bismuth exposed-core fiber has a maximum fluorescence capture of 5.7% into the mode with polarization parallel to the axis of symmetry, which is greater than the fully filled case (4.7%), but only 4.0% into the orthogonal mode. This difference is due to the presence of a high intensity peak in the sensing region for the fundamental mode with polarization parallel to the axis of symmetry, which is absent for the orthogonal mode.

To directly compare the difference in fluorescence capture between the fully filled and exposed-core fibers the FCF curves for each fundamental mode are added as required by Eq. (3), with the results presented in Fig. 5(b). The results for the exposed core fiber are essentially a modification to that of the fully filled fiber where there is potential for enhancing the fluorescence capture by moving to the asymmetric geometry. Figure 5(b) shows that, for particular core diameters, FCF is greater for the exposed-core design by as much as 29% for silica fibers and 19% for F2 fibers, at their respective optimum core diameters.

To understand this effect, NOI (Eq. (4)) was evaluated and is presented in Fig. 6. We see that before the point where the modes spread out dramatically into the water filled hole there is little difference in NOI values between the two fiber designs and hence most of the behavior can be explained in terms of the effective area. The reduced effective mode area of the exposed-core fiber compared with the fully filled fiber is due to the stronger confinement at the air-glass boundaries and accounts for the observed FCF. However, there is little increase in FCF for the exposed-core Bismuth fiber because of the small relative difference between the air-glass and water-glass ratios. The refractive index of water is much closer to that of silica, and hence we see the greatest improvement in the lower refractive index glasses.

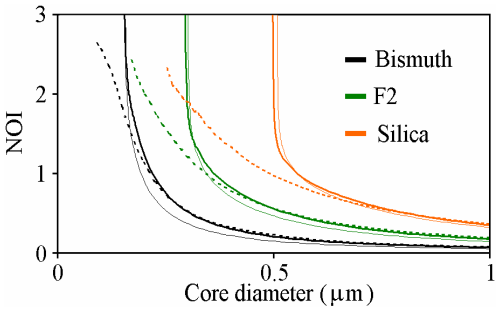

Fig. 6. Normalized overlap integral (NOI) as a function of core diameter for three substrate glasses (indicated in legend), where the fiber is either fully filled with water (dashed) or is an exposed-core fiber with one hole containing water (solid). The thick solid lines refer to the fundamental mode of the exposed-core case that is polarized parallel to the axis of symmetry and the thin line is for the fundamental mode with orthogonal polarization.

5. Coupling efficiency

There are two main coupling problems that need to be considered in the design of the class of sensor considered in this paper. The first is input coupling of an excitation source into the fiber which, although different for different fiber geometries, has largely been dealt with by other authors (for example, see [21, 28-32]). Coupling into small-core optical fibers is by no means trivial; however, the exact efficiency is largely system dependant. A more fundamental (and unavoidable) issue is the loss associated with the mode mismatch between empty regions of fiber and regions along the fiber that are locally immersed within a liquid. For systems where several locations are to be sensed, these liquid interface losses are multiplicative and thus these losses may become significant.

To evaluate the losses associated with this mode mismatch we enforce the continuity of the transverse components of electric and magnetic fundamental modes, which can be expressed as Eqs. (5) and (6),

$$\hat{\vec{E}}_{t1} + a\hat{\vec{E}}_{t1} + b\hat{\vec{E}}_{t2} = a'\hat{\vec{E}}'_{t1} + b'\hat{\vec{E}}'_{t2} + \vec{E}_{rad} \tag{5}$$

$$\hat{\vec{H}}_{t1} - a\hat{\vec{H}}_{t1} - b\hat{\vec{H}}_{t2} = a'\hat{\vec{H}}'_{t1} + b'\hat{\vec{H}}'_{t2} + \vec{H}_{rad} \tag{6}$$

where $|a|^2$, $|b|^2$ and, $|a'|^2$ and $|b'|^2$ are the reflected and transmitted coupling efficiencies into the two fundamental modes (subscripts *1* and *2* respectively), *rad* refers to the transmitted radiation field and *t* refers to the transverse components of the electric and magnetic fields. We vector multiply Eqs. (5) and (6) by the conjugated magnetic and electric fields respectively, integrate over an infinite cross section and use orthonormality of the fiber's guided and radiation modes to obtain a matrix equation for *a*, *b*, *a'* and *b'* involving cross integration terms between all four fundamental modes (two for each the filled and unfilled sections of fiber). Assumed in this approach is that the reflected light distribution at the boundary is directly proportional to the fundamental guided modes, that is, that reflection into the radiation modes is negligible [1, 33].

The liquid interface losses were determined for the case of an exposed core fiber being immersed into an aqueous solution and a corresponding WW fiber with three holes filled. These losses consist of both excitation light coupling from the unfilled region into the water containing region and then the reverse at the fluorescence wavelength (Fig. 7). Note that this analysis is appropriate for both forwards and backwards detection of fluorescence, that is, whether measuring the fluorescence from the distal end or pump end of the fiber. The results are shown in Fig. 8(a) for transmission through the boundaries of a single segment of the fiber filled with water.

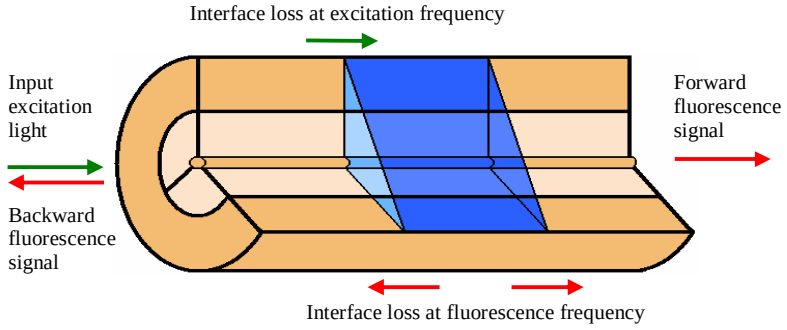

Fig. 7. Schematic of an exposed-core fiber with a section immersed in a liquid. Liquid interface losses exist for the excitation light entering the liquid filled section and for the fluorescence exiting the liquid filled section.

For both fully filled and exposed core fiber sensors, the liquid interface losses increase for small core diameters due to the increased amount of optical power in the cladding holes. Comparing the two sensing fiber designs considered here, we see that the liquid interface losses are relatively better for exposed-core fibers compared with the fully filled equivalent when large core diameters (c.f. wavelength) are used, since only one of the cladding holes is filled and therefore the geometry more closely matches the unfilled section of fiber. However, as the core diameter decreases, the exposed-core fiber experiences dramatically enhanced guidance within the single filled hole, which deforms the mode profile compared with the unfilled fiber and thus rapidly reduces transmission across the liquid interface. This, along with the above fluorescence capture results (Sec. 4), demonstrates that care must be taken in choosing a core diameter for an exposed-core fiber, as core diameters that are too small (less

than 0.16μm for bismuth and less than 0.50μm for silica) result in both significant liquid interface losses and a reduction in FCF.

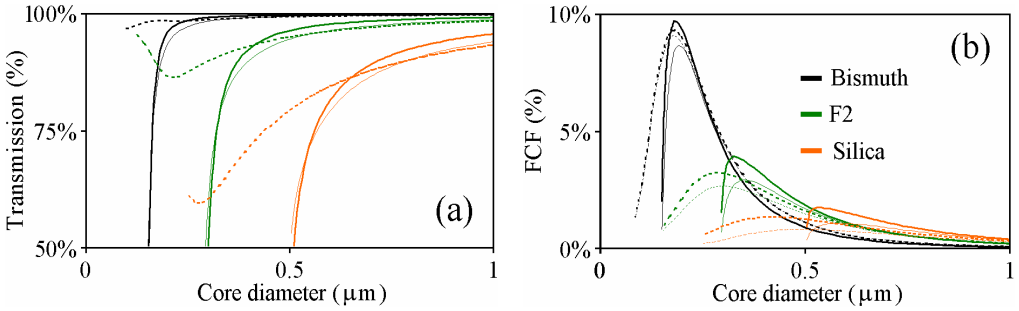

Fig. 8. Liquid interface transmission for a single coupling in and out event corresponding to one fluid-filled region (a) and FCF multiplied by this transmission (b), as a function of core diameter for three substrate glasses (indicated in legend). The fiber is either fully filled with water (dashed) or is an exposed-core fiber with one hole containing water (solid). In (a) the thick solid lines refer to the first fundamental mode of the exposed-core case and the thin line is for the second fundamental mode. In (b) the thick lines refer to FCF without considering liquid interface losses whereas the thin lines include the appropriate liquid interface losses where each non-degenerate mode of the exposed-core fiber has been considered separately.

Figure 8(b) shows the effect on the FCF results of Fig. 5(b) when liquid interface losses into and out of a single filled section of fiber are considered, as given by Eq. (7), where n (the number of boundaries the excitation light must travel through to reach the fluorescent region) and m (the number of boundaries the fluorescence must travel through to reach the output of the fiber) have been set to n=m=1. LIT refers to the liquid interface transmission, that is, the fraction of optical power that is not lost by the respective fundamental modes across the liquid interface.

$$FCF_{j,\,final} = \sum_{\nu} (LIT_{E_j})^n \times (LIT_{F_\nu})^m \times FCF_{j\nu} \qquad (7)$$

We see that for bismuth fiber there is no longer an improvement in the exposed-core fiber relative to the fully filled fiber, whereas the lower index glasses are still predicted to enable a significant improvement in fluorescence capture. However, the maximum achievable fluorescence capture is still significantly greater for the high index glasses, regardless of which geometry is chosen and thus we conclude that the exposed-core fiber will still provide highly efficient fluorescence sensing in the small core, high refractive index regime.

In fact, if we consider a long distributive sensor with multiple locally-immersed sections, the advantage of using higher refractive index materials becomes evident. Consider, for example, a fluorescence-based distributive sensor where we wish to receive individual fluorescence signals from multiple sites along the length of the fiber in order to obtain spatial information using methods analogous to optical time domain reflectometry [34]. If we have, say, 5 liquid immersed sections, the excitation light must pass through nine boundaries to reach the final fluorescence region (n=9) and then the fluorescence from this section of fiber will have to propagate back through the same nine boundaries (m=9). These liquid interface losses associated with receiving fluorescence from the fifth liquid-immersed segment are shown in Fig. 9.

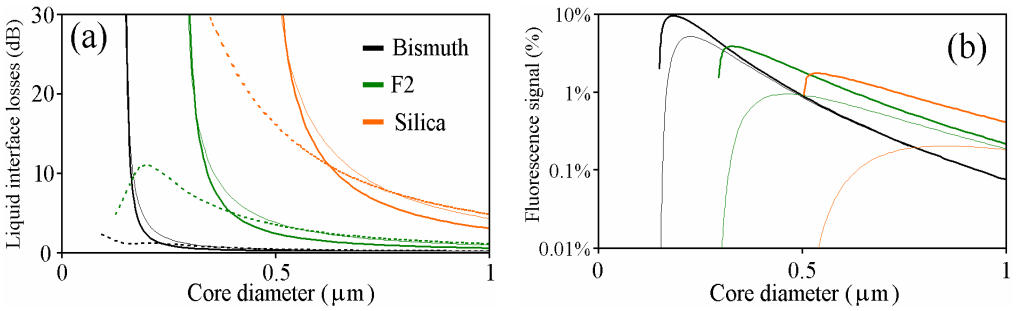

Fig. 9. Liquid interface losses for nine coupling in and out events (m=n=9) as a function of core diameter for three substrate glasses (indicated in legend) (a) and the effect on the fluorescence signal received from the far-end of the fiber (b). The liquid interface losses are associated with five fluid-filled regions, where the fiber is either fully filled with water (dashed) or is an exposed-core fiber with one hole containing water (solid). In (a) the thick solid lines refer to the first fundamental mode of the exposed-core case and the thin line is for the second fundamental mode. In (b) the thick lines refer to FCF without considering the effect of liquid interface losses whereas the thin lines do.

Here we see that the use of a small-core silica fiber introduces large losses, to the order of 10dB and greater for very small cores. In contrast, the bismuth small-core fibers experience very little liquid interface losses, such as less than 5dB for core diameters greater than 0.19μm, which is still in the regime of enhanced fluorescence capture. The effect on FCF, shown in Fig. 9(b), is again highlighted. Relatively small liquid interface losses allow the high refractive index glasses to still provide a high fluorescence signal (5% maximum for bismuth at a core size of 0.22μm) whereas the silica fiber provides a much reduced fluorescence signal (0.2% maximum at a core diameter of 0.85μm).

6. Discussion and conclusions

Exposed-core microstructured fibers have been theoretically studied to determine their potential for the use in both absorption and fluorescence based sensing and have been compared to an equivalent fully filled fiber. In particular, exposed-core liquid-based sensors are shown to enable several optical advantages due to the presence of a raised refractive index in the sensing region. These allow the exposed-core fiber to compete with a fully filled fiber as a sensor, despite utilizing only one-third of the cladding holes (in this particular implementation). Firstly, the amount of available optical power in the sensing region of an exposed-core fiber can compete with other liquid-filled MOF-based sensors due to the spreading of the mode into the sensing region. Secondly, the exposed-core fiber can provide an enhancement in fluorescence capture ability such as an increase of 19% for lead silicate fibers and 29% for silica fibers. To further consider the working characteristics of an exposed-core fiber, and any liquid filled fiber, we have also calculated the coupling losses that are introduced due to the presence of the liquid's refractive index. We have shown that while these coupling losses are present, they do not degrade the sensitivity significantly for fiber dimensions of interest, particularly where high refractive index materials are used. When considering the effects of both coupling efficiency and fluorescence capture together we have seen that small-core high refractive index glasses offer an enormous benefit in sensitivity, regardless of whether using an exposed-core or fully filled fiber.

Of course, in order to implement an exposed-core fiber in a real sensing application there are several practical issues that need to be solved. First and foremost is fiber fabrication; while several examples of exposed-core fibers have now been fabricated there is still considerable room for improvement on insertion loss (of the exposed section), fiber length, and fiber quality. Another important consideration is the coupling efficiency and stability into small-core fibers, which must be solved before sensor implementation can be made reliable and accurate. The are also application specific considerations for absorption and fluorescence

based sensors such as the choice of absorption or fluorescence material, sources, and detectors, which must all be considered in a practical system.

However, given the potential for distributive sensing, no requirement for filling, and these predicted sensing characteristics, it can be expected that exposed-core fibers will provide new opportunities for optical fiber-based sensing.

Acknowledgments

The authors acknowledge the support of the Defence Science and Technology Organisation (DSTO), Australia and in particular the DSTO Corporate Initiative on Smart Materials and Structures for sponsorship of this program of research. This research was supported under the Australian Research Council's Discovery Projects funding scheme (project number DP0665486)